

Direct measurement of ballistic to diffusive crossover in colloidal particles in simple and complex fluids

Andrew P. Hammond, Eric I. Corwin

Materials Science Institute and Department of Physics, University of Oregon, Eugene, Oregon 97403

(Dated: January 26, 2017)

A thermal colloid suspended in a liquid experiences two types of motion. At short time scales the motion will be ballistic and at long time scales diffusive. We directly observe a free floating tracer particle's motion in both regimes and its transition between the two. By analyzing the motion of the tracer particle in a dense Newtonian fluid, we measure the temperature, viscosity, and tracer radius. In addition, the full transition gives us added insight into the structure of the fluid. We confirm this by examining a tracer's motion in a non-Newtonian Maxwell fluid. We find a significant shift in the transition between ballistic and diffusive motion with the addition of intermediary thermal spring like motion. The Maxwell transition also shows an increase in the effective mass of the tracer particle.

At very short time and length scales the diffusive motion of a Brownian particle breaks down into a series of individual ballistic flights. At a time when it was impossible to contemplate the direct imaging or observation of individual molecules, this idea was used by Einstein as definitive proof for the molecular composition of fluids [1]. Indeed, the microscopic time and length scales for the ballistic motion are so small that direct measurements have only recently become possible [2–5]. These experiments have used optical traps to confine a test particle within a harmonic well, allowing a high precision measurement of the short time motion but at the cost of a loss of information about the crossover to diffusive behavior. Here we present direct measurements of the full transition between ballistic and diffusive motion for a freely moving colloid suspended in simple Newtonian and complex Maxwell fluids. These measurements are achieved using a high speed camera, intense illumination, and an accurate tracking algorithm [6]. These measurements have sufficient precision to unambiguously distinguish between microscopic models for fluids [7–14]. In a simple Newtonian fluid we find that nearby fluid is frictionally bound to the particle, increasing its effective mass. By contrast, in a complex Maxwell fluid made up of interacting micelles the region of bound fluid is much greater leading to an even larger effective mass. The functional form of the full transition provides a direct measurement of the temperature and rheological response of the fluid.

In this experiment we directly measure the mean squared displacement (MSD) of a freely floating colloid in simple and complex fluids. We examine a free floating unperturbed polystyrene test particle with a radius of $21.8 \mu\text{m}$ (Spherotech, ppx-400-10). We place the particle in either density matched salt water, a Newtonian fluid, or a density matched Cetyltrimethylammonium chloride (CTAC) and water solution, a non-Newtonian Maxwell fluid. Our fluid sample is isolated from external influences inside of a silicon well sandwiched between a glass slide and cover slip. Using a high speed camera (Vision Research Miro 310) we image the motion of the particle

at a frame rate of 40,000 frames per second, yielding a minimum lag time between measurements of $25 \mu\text{s}$. We track the particle's motion with nanometer accuracy as shown in figure 1.

A rigorous theoretical framework connecting fluid properties to the observable MSD of a colloid is provided by solving the Langevin equation of state. The simplest model for a fluid is the ideal gas [15, 16] whose Langevin equation has only two terms. The MSD for an ideal gas has two asymptotic behaviors, at long times it is diffusive ($\text{MSD} \propto t$) and at short times ballistic ($\text{MSD} \propto t^2$). The transition between these two behaviors is exponential, and thus rapid.

A more sophisticated model for dense fluids, motivated by early computer simulations [17, 18], is achieved by adding an effective mass term and a memory term to the ideal gas model [7, 9]. The effective mass term models the frictionally bound fluid that is attached to the particle and the memory term models the inertial interaction of the particle with nearby moving fluid [19]. At sufficiently short timescales and close to the speed of sound in the fluid this model breaks down and is replaced with the simple ideal gas model.

These modifications to the Langevin equation were analytically solved [10] under the assumptions that the fluid is viscous and incompressible, the Reynolds number is low, and the test particle is a hard sphere [8, 20]. The predicted MSD is included in the supplementary information. The dense fluid MSD differs from the ideal gas MSD in two salient ways: 1) It gives rise to a slower ballistic velocity, caused by the increased effective mass of the particle. 2) It has a much gentler crossover between ballistic and diffusive motion, caused by the inertial memory of the liquid.

Non-Newtonian fluids, however, can have much more complicated Langevin equations [11, 12]. One of the simplest non-Newtonian fluids is a Maxwell fluid, characterized by a single relaxation time between spring like and viscous like behavior. This thus requires the addition of a decaying spring term to the Langevin equation. This

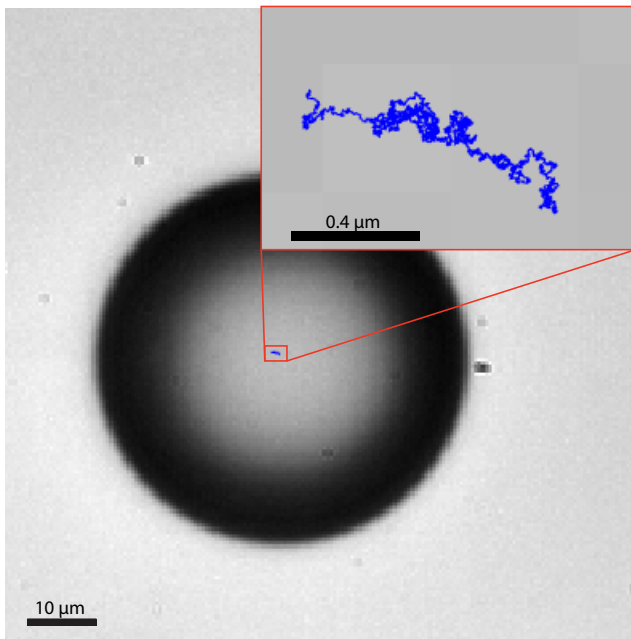


FIG. 1. A single colloid suspended in water viewed through the microscope. The path the particle travels for the next 2 seconds is shown in blue.

additional term makes a closed form MSD difficult to solve for, but we expect the addition of an intermediate plateau regime in the MSD corresponding to the behavior of a thermal spring.

In this experiment, we used polystyrene hard spheres with a radius of $21.8 \mu\text{m}$ as our tracer particle. Polystyrene was chosen because it is easily density matched to water using NaCl with only minimal, and known, changes to the viscosity. The size of the particle, much larger than those in optical trap experiments, was chosen because the tracking precision as well as the ideal gas transition time and length increase with increasing radius. We chose to use water as our experimental liquid because of its ubiquity in experiments and its relatively low viscosity. For our setup, the Reynolds number is 2.4×10^{-9} . This system fulfills all of the underlying assumptions required by the dense fluid equation. When selecting a Maxwell fluid we chose to use a solution of Cetyltrimethylammonium chloride (CTAC) mixed with water. This mixture has been found to exhibit a Maxwell fluid behavior caused by worm-like micelles [12, 21] and is a commonly studied Maxwell fluid. Fortunately, at the concentrations where a Maxwell behavior is exhibited, the solution has a density range which overlapped the tracer particle density.

Test particles were placed into a deionized water mixture at $5 \times 10^{-3} \%$ w/v of colloid. The colloids are slightly denser than water, so NaCl was added to density match the system at a measured value of $1.06 \times 10^3 \text{ kg/m}^3$. After sonicating and degassing the colloid-water solution,

it was placed in a Fastwell silicon spacer cavity between a slide and a cover slip. The chamber was sealed with vacuum grease to ensure that there were no air bubbles. The silicon spacer had a width of 2.4 mm and circular void with a radius of 5 mm allowing the colloids to be imaged far from wall effects. The slides were cleaned with piranha solution and dried with nitrogen gas, which removed any coatings on the slides.

For the Maxwell fluid, we added the same polystyrene beads to CTAC at a concentration of $2.5 \times 10^{-3} \%$ w/v. The fluid density was measured to be $1.055 \times 10^3 \text{ kg/m}^3$ slightly lower than the average density of the beads. However, the density is close enough that beads did not fall out of suspension until well after the measurements were complete. When preparing samples, we used a process almost identical to the one for water. The major difference was that the sample was not sonicated or mixed ahead of being added to the Fastwell because the fluid acted solid-like when exposed to high frequency agitation. Instead, the sample was slowly mixed using a low frequency mixer.

All data was collected on a Nikon TE2000s microscope on a floating stage optical table in a climate controlled room. Illumination was provided by a 500mW red LED (Thorlabs LED635L) shining through the microscope condenser. In between the LED and sample a neutral density filter on a swivel mount was added to allow initial setup to be done without excessive local heating of the sample. The sample was encased in a small cardboard box for isolation from acoustic vibrations. Images were gathered through a 50x lens (Nikon LU plan ELWD 50x/0.55 B inf/0 WD 10.1) using a Phantom M310 high speed camera. Videos were taken at 40,000 fps ($T = 25 \mu\text{s}$) with an image size of 192x192 pixels and a magnification of $0.4 \mu\text{m}/\text{pix}$. When filming a particle all motorized elements on the microscope and camera were turned off to eliminate small vibrations. Once a particle was found, filming lasted 2.84 s (113,600 frames) after which the LED was immediately shut off and the ND filter replaced.

We used a radial center tracking algorithm[6] to find the center of the colloids in progressive frames of the video. Using a combination of simulations and tracking test particles which were stuck to the slide, we found that the algorithm did not exhibit a preferred direction. We found that the mean position error was about 1.5 nm in each frame.

We calculate the MSD from our measured data as $\text{MSD}(\tau) = \langle \|\vec{x}(t+\tau) - \vec{x}(t)\|^2 \rangle$ where $\vec{x}(t)$ is the measured position of the particle at time t , τ is the lag-time between position measurements, and angle brackets denote a time average. The MSD for a representative particle is plotted as green squares in figure 2. This MSD exhibits a small drift at long times, past about 0.1 s, and a noise floor at very short times. The drift is likely the result of convective flows within our sample chamber,

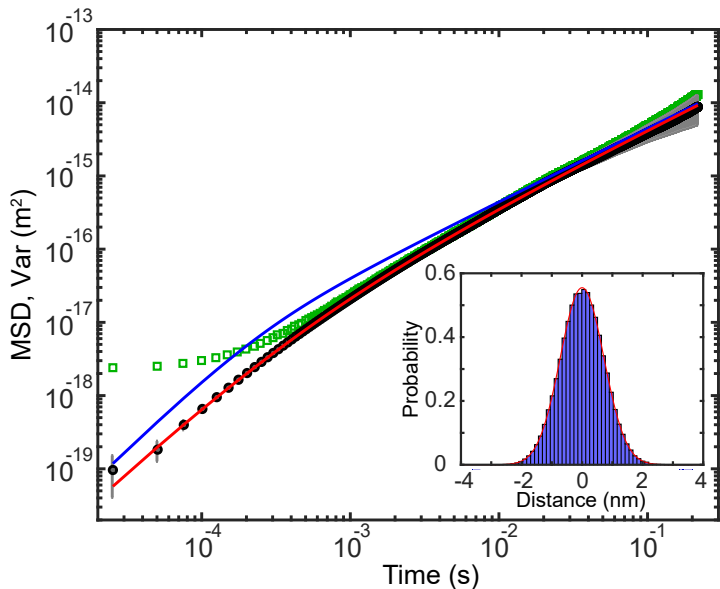


FIG. 2. The variance of the colloid's trace, shown in figure 1. The green squares show the mean squared displacement. The black dots with the error bars show the variance with the noise floor subtracted, in this case $2.34 \times 10^{-18} \text{ m}^2$. In red is the dense fluid MSD fit with Temperature 302 K, radius $21 \mu\text{m}$. For comparison, the ideal gas prediction is plotted in blue with diffusive asymptote matching the data. The ideal gas uses the same fitting parameters as the dense fluid fit. We propagate the localization error of the position measurement as well as sampling error through our calculation to obtain error bars for the plot as described in the supplementary material. Inset: A histogram of measured positions for a stranded particle.

driven, perhaps, by local heating of the sample. However, this drift can be easily removed by calculating the variance of particle position as a function of lag time as $\text{Var}(\tau) = \text{MSD}(\tau) - \|\langle \vec{x}(t+\tau) - \vec{x}(t) \rangle^2\|$. The noise floor is caused by photon shot noise in our camera contributing to uncertainty in the localization of a particle. We can directly measure this noise by tracking a particle fixed to a slide and find it to be independent and identically distributed Gaussian noise with a variance of approximately $2 \times 10^{-18} \text{ m}^2$ (inset to figure 2). The precise value of this noise variance changes from run to run due to variations in particle size and particle focus (due to changes in z-position). Because this noise is independent and identically distributed for a given measurement we can simply subtract the noise floor from our measurement to find the true variance of our particle, plotted as black circles in figure 2.

The plotted variance clearly shows a ballistic regime below about 10^{-3} to 10^{-4} s , a crossover regime up till about 10^{-2} s , and a diffusive regime for longer times. As expected, when plotted against the ideal gas model matching the diffusive asymptote it is immediately clear that it does not describe the behavior of our system,

shown in blue in figure 2. The dense fluid model, however, fits exceedingly well over the entire range of measured lag-times. The model depends on four physical parameters: 1) temperature, 2) particle radius, 3) fluid density, and 4) fluid viscosity. Of these, we independently measure the fluid density prior to observation. The fluid viscosity of salt water is a known function of density and the temperature [22]. Therefore, we have only two independent fitting parameters: temperature and particle radius. To this, we add a third fitting parameter to describe the magnitude of the noise floor.

We independently fit 18 measurements using 18 different particles, shown in figure 3. On average, the particle radius was found to be $20.5 \pm 0.8 \mu\text{m}$, within tolerance of the manufacturer's quoted radius. The average temperature measured by our fitting was found to be slightly higher ($297 \pm 4.5 \text{ K}$) than the measured room temperature ($293 \pm 2 \text{ K}$), likely the result of local heating from the intense illumination. The noise floors for the measurement were found to range from $1.2 \times 10^{-18} \text{ m}^2$ to $2.4 \times 10^{-18} \text{ m}^2$. Thus fit, the dense fluid functional form is indistinguishable from the data over much of our measured range. To characterize the agreement, we plot the residual percentages, and find them to be unbiased and with error less than 5% over at least two decades of lag time, as shown in figure 3. At longer times, where drift and sampling errors increase, the percent error increases as well.

We perform similar experiments in a Maxwell fluid created with a solution of CTAC and water as described in the methods section. This solution has been found to exhibit viscoelastic behavior characteristic of worm-like micelles [12, 21]. Following the procedure outlined in the methods section, we calculated an MSD for a particle suspended in this fluid, shown with green squares for a representative trial in figure 4. As in the case with water, we see a minimum noise floor at short times and a long time drift. The drift in the measurement can be removed by using the variance as described above. The noise floor can also be estimated and subtracted to calculate a true variance for a particle within a CTAC fluid.

The plotted variance for a Maxwell fluid, of which a characteristic example is shown in figure 4, has three notable features. First, at short times the motion is clearly ballistic. The best fit prefactor for the asymptote is however considerably lower than the one predicted by either the ideal gas or dense fluid models, corresponding to an effective mass four times larger than the particles mass or an entrained region of radius $33 \mu\text{m}$. This increased effective size of the particle can be understood using the fact that the surrounding fluid contains worm-like micelles. The micelles in contact with the test particle effectively form tentacles stretching off into the fluid, thus extending the effective radius. Second, the variance shows a clear secondary plateau which is independent of the noise floor. This plateau is characteristic of thermally damped mo-

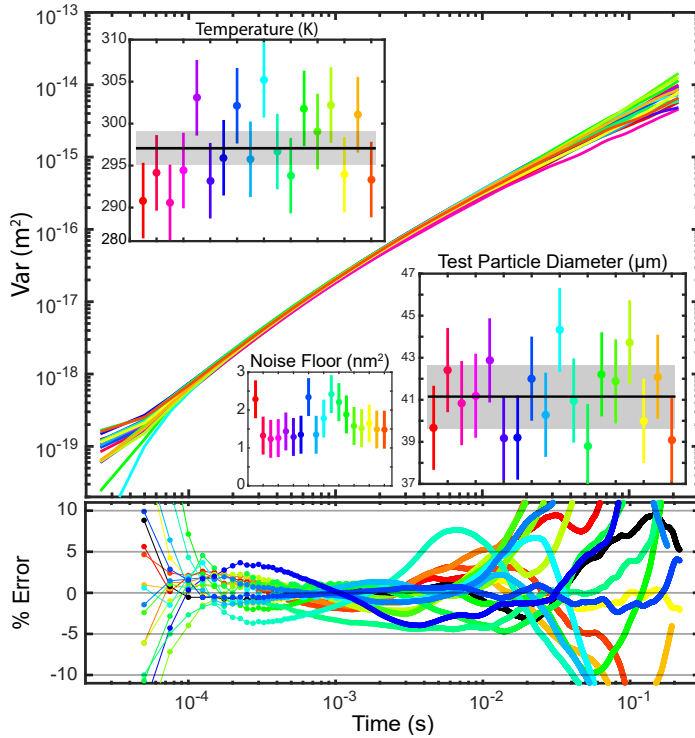


FIG. 3. Top: The noise floor adjusted variance for 18 different videos. Inset: The fitted temperature, test particle radius, and noise floor for the different trials. The black line shows the mean values with a grey standard deviation. Bottom: Residual percentages showing by what percent the measurement deviates from the individual fits for each of the corresponding variance's shown above.

tion consistent with a Maxwell fluid's predicted behavior for high frequencies. Finally, for long times, near the end of the variance there is movement away from the plateau indicative of the beginning of the transition to diffusive motion.

In this experiment, we resolve the functional form of the ballistic-diffusive crossover which reveals the fundamental length and time scales between individual and collective interactions in both Newtonian and Maxwell fluids. In so doing we have created a microscale first-principles thermometer based on the kinetic theory definition of temperature. This method allows for extracting rheological information at extremely high frequencies from single particle motion, as it is performed at a microscopic scale with correspondingly high spatial resolution whereas rheometers are necessarily macroscale. These results provide an independent method for testing the models for the microscopic structure of dense fluids. This method demonstrates the ability to measure multiple transitions between dominant effects in viscoelastic materials, an area where laser traps have difficulty because of the effects of confinement [23]. This method is also able to examine the influence of long range interactions, such as wall effects, without interference from the

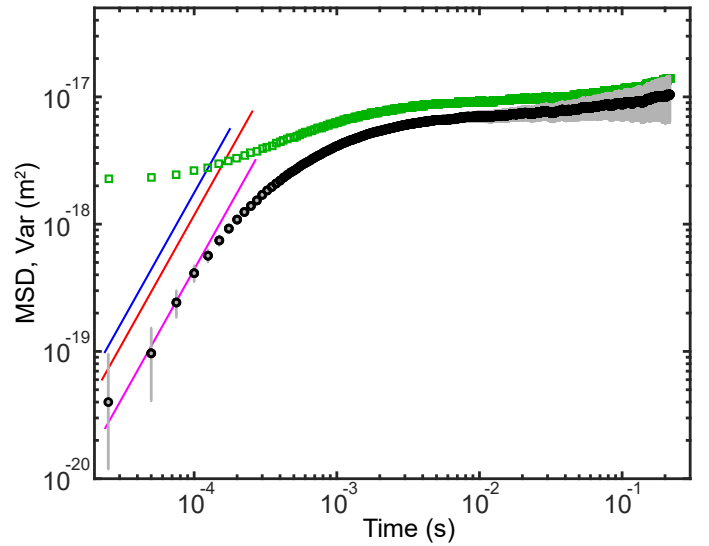


FIG. 4. The MSD and adjusted variance for a particle moving in a Maxwell fluid. The green squares show the unadjusted MSD. The black dots show the noise floor subtracted variance. In this figure the noise floor used is $2.2883 \times 10^{-18} \text{ m}^2$. The blue, red and magenta lines are the ballistic asymptotes corresponding to the ideal gas, dense fluid, and fit respectively.

laser trap [24]. As such, high speed single particle tracking promises to become an important tool in the study of the fundamental structure of liquids.

We thank Raghu Parthasarathy, Tristan Ursell, and Mike Taormina for helpful discussions. We also thank the University of Oregon machine and electrical shop staff. This work was supported by National Science Foundation (NSF) Career Award DMR-1255370.

-
- [1] A. Einstein, Ann. Phys. **322**, 549 (1905).
 - [2] B. Luki, S. Jeney, C. Tischer, A. J. Kulik, L. Forr, and E.-L. Florin, Phys. Rev. Lett. **95**, 160601 (2005).
 - [3] R. Huang, I. Chavez, K. M. Taute, B. Luki, S. Jeney, M. G. Raizen, and E.-L. Florin, Nat Phys **7**, 576 (2011).
 - [4] T. Franosch, M. Grimm, M. Belushkin, F. M. Mor, G. Foffi, L. Forr, and S. Jeney, Nature **478**, 85 (2011).
 - [5] S. Kheifets, A. Simha, K. Melin, T. Li, and M. G. Raizen, Science **343**, 1493 (2014).
 - [6] R. Parthasarathy, Nat Meth **9**, 724 (2012).
 - [7] R. Zwanzig and M. Bixon, Phys. Rev. A **2**, 2005 (1970).
 - [8] A. Widom, Phys. Rev. A **3**, 1394 (1971).
 - [9] E. J. Hinch, Journal of Fluid Mechanics **72**, 499 (1975).
 - [10] H. J. H. Clercx and P. P. J. M. Schram, Phys. Rev. A **46**, 1942 (1992).
 - [11] J. H. van Zanten and K. P. Rufener, Phys. Rev. E **62**, 5389 (2000).
 - [12] C. Wilhelm, J. Browaeys, A. Ponton, and J.-C. Bacri, Phys. Rev. E **67**, 011504 (2003).
 - [13] M. Atakhorrami, D. Mizuno, G. H. Koenderink, T. B. Liverpool, F. C. MacKintosh, and C. F. Schmidt, Phys.

- Rev. E **77**, 061508 (2008).
- [14] Y. L. Raikher, V. V. Rusakov, and R. Perzynski, *Soft Matter* **9**, 10857 (2013).
 - [15] D. S. Lemons and A. Gythiel, *American Journal of Physics* **65**, 1079 (1997).
 - [16] G. E. Uhlenbeck and L. S. Ornstein, *Phys. Rev.* **36**, 823 (1930).
 - [17] A. Rahman, *The Journal of Chemical Physics* **45**, 2585 (1966).
 - [18] B. J. Alder and T. E. Wainwright, *Phys. Rev. A* **1**, 18 (1970).
 - [19] R. Zwanzig and M. Bixon, *Journal of Fluid Mechanics* **69**, 21 (1975).
 - [20] L. D. Landau & E.M. Lifshitz, *Fluid Mechanics* (Pergamon Press, 96-98, 1959).
 - [21] R. Oda, J. Narayanan, P. A. Hassan, C. Manohar, R. A. Salkar, F. Kern, and S. J. Candau, *Langmuir* **14**, 4364 (1998).
 - [22] M. H. Sharqawy, J. H. L. V, and S. M. Zubair, *Desalination and Water Treatment* **16**, 354 (2010).
 - [23] M. Grimm, S. Jeney, and T. Franosch, *Soft Matter* **7**, 2076 (2011).
 - [24] B. U. Felderhof, *The Journal of Chemical Physics* **123**, 184903 (2005).